Improved confinement in high-density H-modes via modification of the plasma boundary with Lower Hybrid RF

PSFC/JA-14-29

Improved confinement in high-density H-modes via modification of the plasma boundary with Lower Hybrid RF

Terry, J.L., Reinke, M.L.[*], Hughes, J.W., LaBombard, B., Theiler, C.[**], Wallace, G.M., Baek, S.G., Brunner, D., Churchill, R.M.[***], Edlund, E.[***], Ennever, P., Faust, I., Golfinopoulos, T., Greenwald, M., Hubbard, A.E., Irby, J., Lin, Y., Parker, R.R., Rice, J.E., Shiraiwa, S., Walk, J.R., Wukitch, S.J., Xu, P., and the Alcator C-Mod Team

November 2014

Plasma Science and Fusion Center
Massachusetts Institute of Technology
Cambridge MA 02139 USA

[*] York Plasma Institute, Department of Physics, University of York, Heslington, York
[**] Ecole Polytechnique Federale de Lausanne (EPFL), Centre de Recherches en Physique des Plasmas (CRPP), CH-1015 Lausanne, Switzerland
[***] Princeton Plasma Physics Laboratory, Princeton, NJ, USA 08543

This material is based upon work supported by the U.S. Department of Energy, Office of Science, Office of Fusion Energy Sciences, under Award Numbers DE-FC02-99ER54512 and DE-AC02-09CH11466 and in part by an appointment to the US DOE Fusion Energy Postdoctoral Research Program administered by ORISE.

Submitted for publication to the *Physics of Plasmas*

Improved confinement in high-density H-modes via modification of the plasma boundary with Lower Hybrid RF

J.L. Terry[a*], M.L. Reinke[a,b], J.W. Hughes[a], B. LaBombard[a], C. Theiler[a,c], G.M. Wallace[a], S.G. Baek[a], D. Brunner[a], R.M. Churchill[a,d], E. Edlund[a,d], P. Ennever[a], I. Faust[a], T. Golfinopoulos[a], M. Greenwald[a], A.E. Hubbard[a], J. Irby[a], Y. Lin[a], R.R. Parker[a], J.E. Rice[a], S. Shiraiwa[a], J.R. Walk[a], S.J. Wukitch[a], P. Xu[a], and the C-Mod Team

[a] *Plasma Science and Fusion Center, MIT, Cambridge, MA, USA 02139*

[b] *York Plasma Institute, Department of Physics, University of York, Heslington, York*

[c] *Ecole Polytechnique Federale de Lausanne (EPFL), Centre de Recherches en Physique des Plasmas (CRPP), CH-1015 Lausanne, Switzerland*

[d] *Princeton Plasma Physics Laboratory, Princeton, NJ, USA 08543*

Abstract

Injecting Lower Hybrid Radio Frequency (LHRF) waves into Alcator C-Mod's high-density H-mode plasmas has led to enhanced global energy confinement by increasing pedestal temperature and pressure gradients, decreasing the separatrix density, modifying the pedestal radial electric field and rotation, and decreasing edge turbulence. These experiments indicate that edge LHRF can be used as an actuator to increase energy confinement via modification of boundary quantities. H_{98}-factor increases of up to ~35% (e.g. H_{98} from 0.75 to 1.0) are seen when moderate amounts of LH power (P_{LH}/P_{tot}~0.15) are applied to H-modes of densities $\bar{n}_e$ ~$3\text{x}10^{20}\text{m}^{-3}$, corresponding to values ~0.5 of the Greenwald density. However, the magnitude of the improvement is reduced if the confinement quality of the target H-mode plasma is already good (i.e. H_{98}^{target}~1). Ray-tracing modeling and accessibility calculations for the LH waves indicate that they do not penetrate to the core. The LHRF power appears to be deposited in plasma boundary region, with a large fraction of the injected power increment appearing promptly on the outer divertor target. There is no evidence that the LH waves are driving current in these plasmas. The LHRF-actuated improvements are well correlated with suppressed pedestal density fluctuations in the 100-300 kHz range. There is also a correlation between the improved confinement and a drop in separatrix density, a correlation that is consistent with previous H-mode results with no LHRF.

PACS: 52.50.Sw, 52.55.Fa, 52.55.-s, 52.40.Hf, 52.35.Ra, 52.35.Hr

Corresponding Author Address: 175 Albany St., Cambridge, MA 02319 USA

Corresponding Author E-mail: terry@psfc.mit.edu

I. Introduction

In the study of fusion-grade plasmas we search for actuators that can provide robust control, improve performance, and/or facilitate study and understanding of important plasma phenomena. Injection of directed lower hybrid range of frequency (LHRF) waves is an example of an actuator for non-inductive current drive (LHCD) and for current-profile control. Ion cyclotron range of frequency (ICRF) heating or by neutral beam injection (NBI) heating at levels above what is needed to cause a transition from L-mode to H-mode confinement are well-known examples of actuators that improve performance (as well as heat the plasma). Unbalanced NBI is an example of an actuator for plasma rotation and allows controlled study of the effects of rotation shear on core transport. The work reported here uses lower hybrid waves that do not penetrate to the core of the target plasmas and are not driving significant current in these plasmas. Instead, the LH power actuates changes in the boundary conditions, leading to global improvements in the plasma performance. Hence we refer to this tool as LHRF rather than LHCD (current drive), and we contend that the LHRF is a valuable actuator in these plasmas both for improving performance and for facilitating study of boundary phenomena.

While we will not review the long history of LH as a *current-drive/current-profile-control* actuator, i.e. LHCD (see for example [1-4] and references therein), we will point to some previous results relevant to the present work in which LH power was used in non-conventional ways to facilitate changes in the plasma. On JFT-2M LH was found to improve confinement, with the improvements attributed to changes in edge potentials and reductions in ExB convection [5]. In Alcator C-Mod experiments aimed at demonstrating off-axis LHCD in low density H-mode target plasmas [6], application of the LH power generally resulted in a drop in plasma density, accompanied by increases in plasma temperature. This was brought about by changes in the H-mode pedestal where decreases in $n_{e,ped}$ and the pedestal density gradient were offset by an increased temperature pedestal, such that the pedestal pressure profile remained roughly constant. Overall global confinement was maintained. Recently on the EAST Tokamak, LHRF was used to mitigate the occurrence of ELMs [7]. This was attributed to the formation of helical current filaments flowing along field lines in the scrape-off layer that were induced by LHRF and resulted in a topology change favorable to ELM mitigation.

It has long been recognized that changes in the boundary plasma can have profound effects on the core plasma. A crucial and consequential example is the pedestal as a boundary condition for the core. Other striking examples are: 1) boundary turbulence as likely mechanism for the Greenwald density limit [8] and 2) recycling affecting core performance, perhaps most clearly demonstrated by the positive effects of Li wall-conditioning in TFTR [9] and NSTX [10]. The phenomenon we describe here is also primarily the result of changes actuated in the edge/boundary plasma and is therefore another example of the boundary affecting the core.

The structure of the paper is as follows: a description of the "target" plasma and the LH system that is used to actuate changes in the target plasma (Section II); a description of the observed changes in confinement and their scalings, as well as changes in the H-mode pedestal and the boundary radial electric field (Section III); what we know about the power deposition of the LHRF (Section IV); a description

in Section V of the changes seen in a quasi-coherent mode that is located at the plasma boundary and of changes in broadband density fluctuations occurring in the edge and scrape-off-layer (SOL); in Section VI we connect the present results with those of previous studies of Enhanced D_α (EDA) H-modes in C-Mod [11,12]. A discussion and summary follow in Section VII.

II. The Lower Hybrid RF System and EDA H-mode on Alcator C-Mod

The lower hybrid system [13] on Alcator C-Mod is designed to investigate advanced, non-inductive operation in plasma conditions relevant to future devices such as ITER. LHCD has proven to be an efficient mechanism for non-inductive operation [3]and current profile control [14] on C-Mod at "low" (in the context of this work) densities ($n_e = 0.4 - 0.8\times10^{20}$ m^{-3}). C-Mod's LH antenna [15] consists of a slow wave launching structure located on the low field side and centered on the mid-plane. The launcher has 64 waveguides arranged in 16 columns and 4 rows. The system operates at 4.6 GHz with a maximum of ~0.9 MW launched from the antenna. A maximum of 0.67 MW (launched) was used in these experiments. The launched wavenumber spectrum is controlled by adjusting the relative phasing between waveguides in the array. For these experiments the launched wavenumber spectrum was asymmetric in the toroidal direction, with most of the power launched in the electron current direction, with the peak of the dominant $n_{||} \equiv ck_{||}/\omega$ lobe equal to 1.9. However, as will be discussed in Section IV, we do not believe that the *launched* spectrum is a critical variable for these experiments, since the LHRF is not accessible to the core of the high-density target plasmas and is not driving current in these plasmas.

High-density EDA H-modes heated by 3.1 to 4.3 MW of ICRF (H minority heating of D majority) served as the target plasmas into which the LHRF was injected. EDA H-mode plasmas have H-mode confinement, but are free of edge localized modes (ELMs) and have pedestals regulated instead by a quasi-coherent oscillation (the QC mode) that also allows for steady-state density and impurity levels [16]. A number of time-traces from a representative discharge are shown in Fig. 1, where the steady-state target EDA H-mode is established around 0.62 s by the 3.5 MW ICRF heating, with LHRF applied for $0.92 < t < 1.25$ s These target plasmas were produced at 5.4 T toroidal field and 0.82 MA plasma current in a lower single null diverted configuration. Central temperatures were 3-4 keV (increased during the LHRF), while the range of line-averaged electron densities was from $2.5 - 3.4 \times 10^{20}$ m^{-3}, with corresponding Greenwald fractions[8] of 0.46 – 0.62. Thus these experiments are performed at essentially the ITER field and RF frequencies, at absolute densities roughly three times those planned for ITER, and at Greenwald densities roughly 60% those for ITER. The experiments were carried out with freshly boronized molybdenum-tile PFC surfaces [17] in order to obtain long-duration steady-state H-modes with relatively low concentrations of high-Z Mo impurity. These plasmas were also seeded with low-Z recycling Ne impurity in order to reduce divertor heat flux[12,18]. (There was little change in the recycling neon flux during the LHRF.) Operationally it was also found that relatively low main chamber neutral pressures (for these plasma densities) were necessary to avoid breakdown in front of the LH launcher, which would in turn cause the control-system to turn off the LH power.

III. Observations of Improved Confinement with Lower Hybrid RF Power Applied to EDA H-Modes

As illustrated in Fig. 1, LHRF power was injected into the high-density H-modes

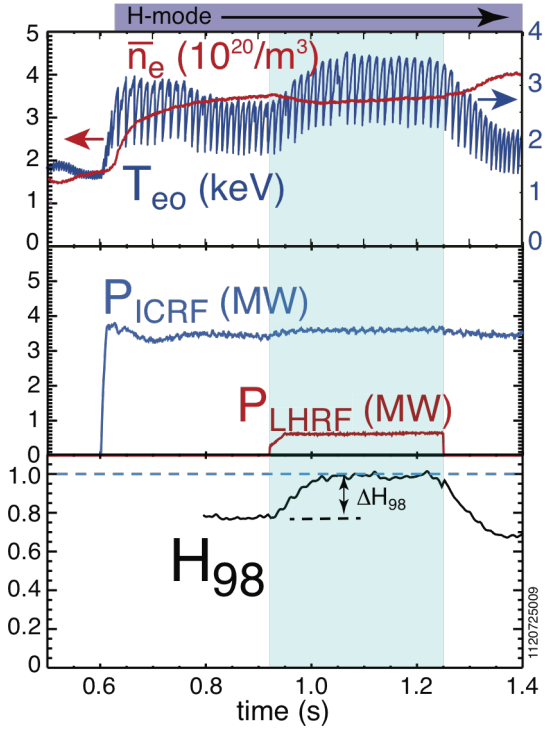

Figure 1. Time histories of line-averaged electron density and central electron temperature (top panel), auxiliary heating powers from ICRF and LHRF (middle panel), and the H_{98}-factor (bottom panel) for a LHRF-actuated higher-density EDA H-mode. The blue shading indicates the time during which the LHRF is on.

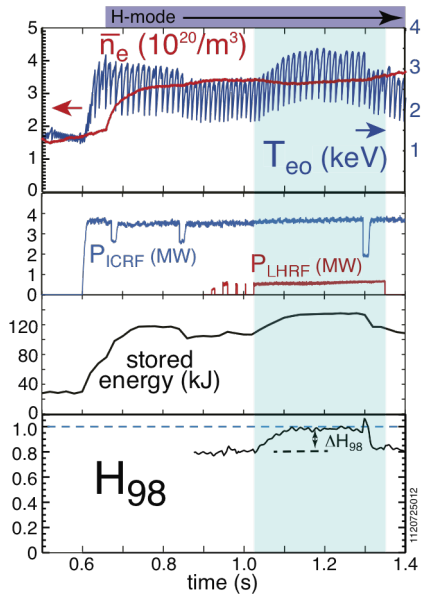

Figure 2. Time histories of line-averaged n_e and central T_e (top panel), ICRF and LHRF heating powers (2nd panel), plasma stored energy (3rd panel), and the H_{98}-factor (bottom panel) for a LHRF-actuated H-mode in which the confinement improvement is lost after an ICRF power drop-out during the LHRF pulse. The improved confinement state did not return the even though the ICRF was restored while the LHRF was still on.

well after steady-state conditions were obtained. For a moderate amount of LHRF power significant increases in plasma stored energy, energy confinement time, neutron rate, T_e, and T_i were observed. The confinement improvements are quantified relative to other tokamaks using the H-factor, H_{98}, which is the energy confinement time, normalized to the multi-machine-based ITER-H98(y,2) scaling law [19]. As seen in Fig. 1, H_{98} increases by as much as 35% when the LHRF is applied. When the LHRF is removed, the drop in H_{98} is often even greater, but the analysis at LHRF turn-off is complicated by evolution of the density and/or radiated power. We note that these changes in H-factor result from changes in confinement time, and not due primarily to changes in the normalizing quantity, $\tau_{ITER\text{-}H98(y,2)}$. It is also the case that the state of improved confinement actuated by the LHRF sometimes ceases before the LHRF turn-off. An example of this is shown in Fig. 2, when a drop-out in ICRF power quenches the effect with the LHRF still on. We have populated a database of those discharges for which the ICRF-heated target plasma is steady before and during the LHRF injection and for which LH power waveform is steady for at least 0.06 s. The confinement analysis assumes that 80% of the launched ICRF power is absorbed by the plasma and that all of the LHRF power is absorbed, the latter being a conservative assumption. The confinement changes are manifested in significant increases in T_e and T_i across the profiles. The electron densities decrease slightly. The core rotation increases in the co-current direction, consistent with the increase in stored energy, but in contrast to prior work where LHRF into lower density H-modes changed rotation in the counter-current direction[6]. The effects on rotation under these conditions are described in more detail in ref [20]. Overall, the major changes to the core plasma temperatures and densities, responsible for the increases stored energy and confinement, are consistent with their responding via profile stiffness to changes occurring in the pedestal. In other words, the core temperature- and density-gradient-scale-lengths, L_{Te} [$=-T_e/(\mathrm{d}T_e/\mathrm{d}r)$], L_{Ti}, and L_{ne} are not changed significantly, but core temperature and density values change to follow the boundary conditions set by the pedestal. The changes in the pedestal profiles wrought by the LHRF injection are illustrated in Fig. 3 for the same discharge whose time traces are shown in Fig. 1. The electron and ion temperatures at the pedestal top increase, while the density there decreases somewhat. However, the electron density *at the separatrix* is reduced significantly, and overall the electron pressure gradient in the pedestal increases by 20-100%. We believe the drop in density at the separatrix to be especially significant and will return to this observation in Section VI.

Before examining the scaling of the changes in H-factor with the LHRF, we digress to explain how the pedestal profiles are obtained. For $T_{e,ped}$ and $n_{e,ped}$, the edge-Thomson scattering (ETS) system measurements[21], taken every 10 ms, are assembled for a 0.07 sec time-interval before the LHRF to yield the pre-LHRF profiles, and assembled for a 0.09 sec time-interval during the LHRF pulse to yield the during-LHRF profiles. The assembled profiles are then fit with a modified tanh function[22]. They are aligned by locating the separatrix at the 100 eV value of the T_e profile fits. Aligning to the same separtrix temperature is justified by power balance

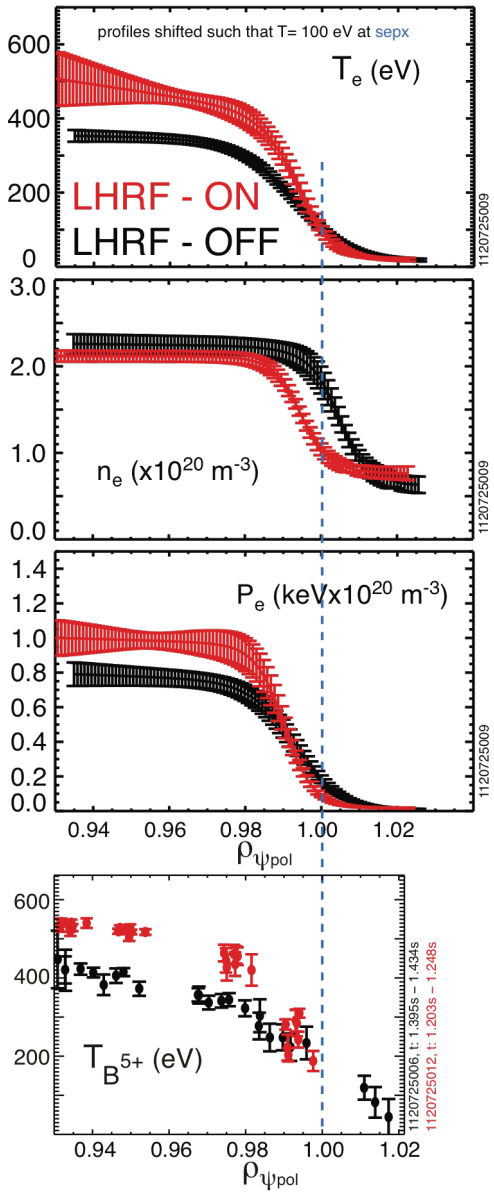

Figure 3. Comparisons of the pedestal profiles of T_e, n_e, electron pressure, and impurity ion temperature (a proxy for T_i) before (black) and during (red) the LHRF-actuated confinement improvement. The electron profiles are modified tanh fits to the measured points and are aligned by placing the separatrix at 100 eV. $T_{imp}(r)$ was measured in a similar discharge and is positioned based on the EFIT mapping.

on the open field lines. The choice of 100 eV for this alignment does not affect significantly any of the conclusions that we draw, with the important demonstration being the inwards shift of the steep gradient region of the *density* pedestal relative to the steep gradient region of the electron temperature. The edge-T_i profile is actually

the temperature profile for the fully-stripped boron impurity ion as measured by the "gas-puff" CXRS system [23]. Its alignment with respect to the ETS profiles has significant (Δr_{sep}~0.014a) uncertainty (unlike the much smaller relative uncertainty among the ETS profiles).

We have examined the dependence of the confinement improvement upon two quantities, with the improvement parameterized by the change in H_{98}-factor from before the LHRF to its maximum value during the LHRF,. The dependence of ΔH_{98} upon the ratio of added LHRF power to the sum of the ICRF and Ohmic power being applied just before the LHRF injection is shown in Fig. 4. A small effect on confinement is seen for LHRF power fractions as low as ~8%, with a rough trend toward larger changes with more LHRF power, at least up to the maximum fraction of 16%. It is also evident in Fig. 4 that there is a range of "improvement" for a given power fraction. Furthermore, it is evident from Fig. 1 that for this discharge the H_{98}-factor of the target plasma is less than 1 and is improved by the LHRF to a value close to 1. This suggests that perhaps the LHRF was "repairing" a less-than-optimal-confinement to one that was limited by other physics and led us to investigate the dependence of improvement upon the H_{98}-factor of the target plasma. This dependence is shown in Fig. 5, and indeed the trend is that the improvement is reduced when the confinement quality of the target H-mode plasma is higher. There are two cases in the data set where the H_{98}-factor is raised significantly above 1 with the LHRF. There is evidence that additional physics is playing a role in these cases, and they will be discussed in Section VII.

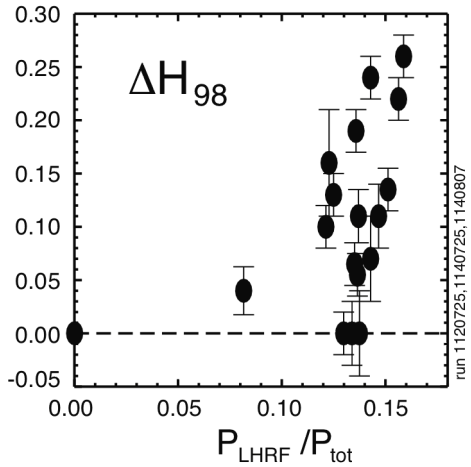

Figure 4. The dependence of the change in the H_{98}-factor brought about by the LHRF as a function of LHRF power normalized by the total power input to the steady-state plasma just before LHRF injection.

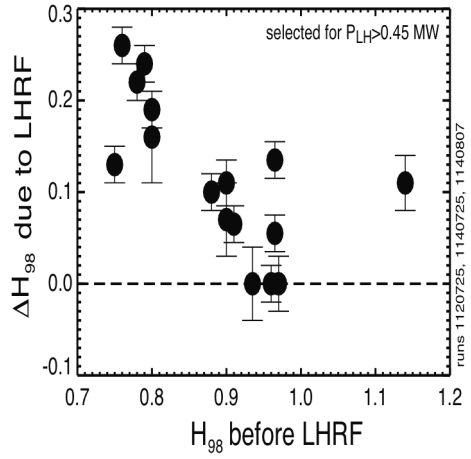

Figure 5. The dependence of the change in the H_{98}-factor brought about by the LHRF as a function of the H_{98}-factor of the target plasma.

Along with the pedestal profiles of T_e, T_i, and n_e, we also have measured profiles of E_r in the pedestal region for two of the improved confinement discharges. $E_r(r)$ is determined [24] by measuring all other terms of the radial impurity force-balance, using the gas-puff-CXRS system. Figs 6(a) and 6(b) each show two E_r profiles, one without LHRF compared to one during LHRF. With the gas-puff-CXRS we did not measure the E_r profile before and during the LHRF on a single discharge. Rather we measured the profile during the LHRF and compared it to a discharge without LHRF that had a similar target plasma produced on the same

day. Fig. 6(a) shows the E_r profile after the confinement was improved from H_{98}=0.80 to 1.0 compared with a no-LHRF target plasma with H_{98}=0.85. Fig. 6(b) shows, on the same scale as 6(a), the E_r profile after the confinement was improved from H_{98}=1.15 to 1.25 compared with a no-LHRF target plasma with H_{98}=1.0. In both comparisons E_r-well appears to shift inward and the E_r-well is deeper during the higher confinement period. The observation that better confined plasmas tend to have a deeper E_r-wells is a general trend for C-Mod discharges [25] and is consistent with the paradigm that **E**×**B** velocity shear suppresses edge turbulence and improves

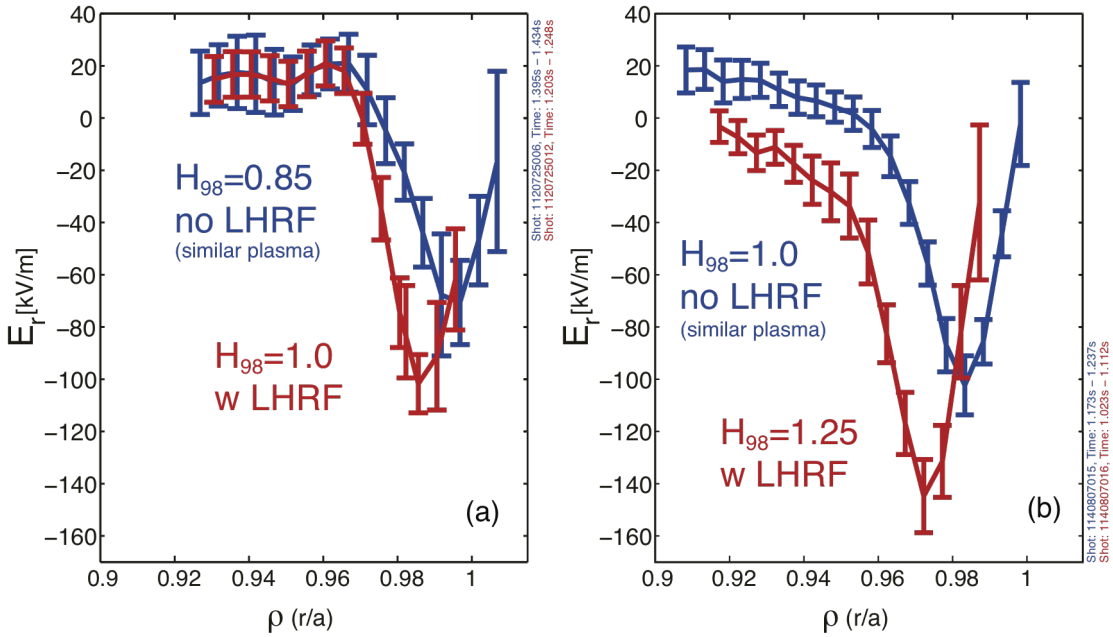

Figure 6. Comparisons of radial electric field profiles in the pedestal for two cases with LHRF-actuated confinement improvements. (6a - in red) for H_{98}=1.0 having been improved from 0.80 and (6b - in red) for H_{98}=1.25 having been improved from 1.15. The blue curves are $E_r(r)$ for discharges without LHRF that were similar to the target plasmas of the LHRF-actuated discharges, i.e. with H_{98}=0.85 (6a – in blue) and with H_{98}=1.0 (6b – in blue).

the transport barrier.

IV. Lower Hybrid RF Power Deposition

Since the plasma modifications are being actuated through changes in the plasma boundary region, we now discuss what is known about the LHRF power deposition. The LH waves are nominally not accessible to the core plasma. The simple criterion[26] for LH waves of frequency ω_0 to be accessible to a region is that the wave $n_{||}$ locally be greater than

$$n_{||crit} \approx \sqrt{1-\frac{\omega_{pi}^2}{\omega_0^2}+\frac{\omega_{pe}^2}{\omega_{ce}^2}}+\frac{\omega_{pe}}{|\omega_{ce}|},$$

where ω_{pi} is the ion plasma frequency, ω_{pe} is the electron plasma frequency, ω_{ce} is the electron cyclotron frequency. This criterion says that waves of $n_{||}$ = 1.9 should not access densities greater than ~0.8x10^{20}m^{-3}. In these target plasmas that density is exceeded everywhere inside the separatrix. Indeed, when we do ray-tracing of the launched LH spectrum with the GENRAY code [27] using the measured temperature and density profiles, we find that this linear model predicts that the waves are mostly absorbed in the SOL plasma on the low-field-side. Because this modeling is ray-

tracing without non-linear effects such as Parametric Decay Instabilities (PDI) (for which there is clear evidence), we cannot assign much certainty to the *details* of the predicted power deposition. (The non-linear effects tend to increase the wave damping.) However, it does provide confidence that most of the LHRF power is absorbed in the boundary region (where "boundary" includes both pedestal and SOL).

We can also obtain knowledge about the LH power deposition by examining the power incident on the outer divertor target surfaces. This is done using IR

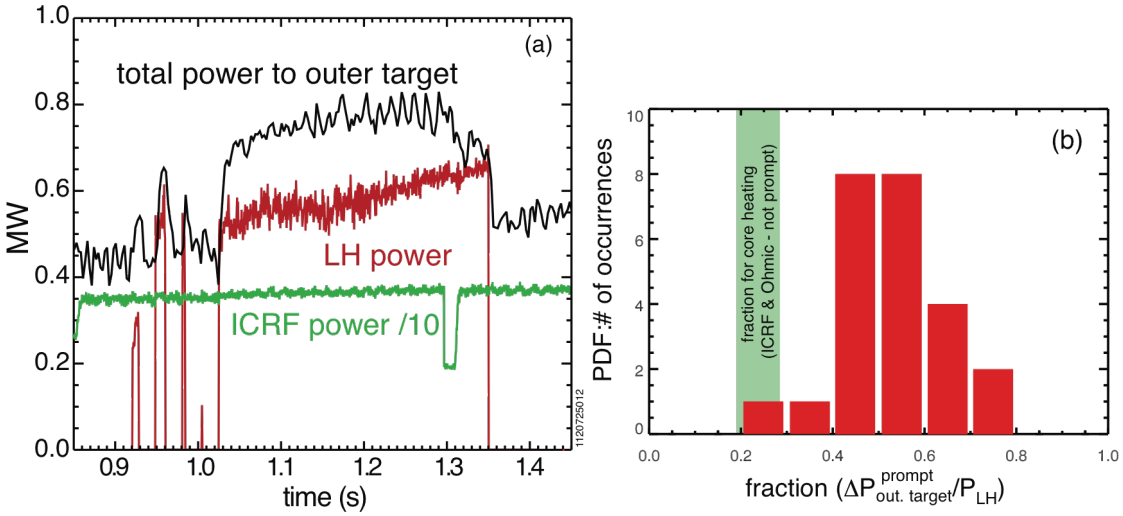

Figure 7. (a) Time response of the total power measured on the instrumented outer-divertor target (black) to the injection of LHRF power (red). Note the prompt response to both the ~0.3 s LH pulse and the three short tripped-out pulses between 0.9 and 1.0 s. Also shown is the waveform of the ICRF power divided by 10 (green). (b) Histogram of the fraction of the LHRF power that shows up promptly on the instrumented outer-divertor (red). This is compared to the typical fraction of core-heating power that shows up on the target for unseeded EDA H-modes.

thermography of an instrumented section of the divertor target [28]. In Fig. 7(a) is shown the response of the total power received on the outer target (assuming toroidal symmetry of the IR thermography measurement), along with the time-histories of the ICRF and LHRF heating powers. As seen, there is a prompt (~5 ms $<< \tau_E$ which is ~35 ms) response to the LHRF power, and the prompt increment in power to the target corresponds to ~40% of the launched LHRF power. A histogram of the number of times a given fraction of the LHRF power appeared promptly (i.e. within tens of ms) on the outer target is shown in Fig. 7(b), along with the fraction of core power (i.e. ICRF plus Ohmic) that typically appears there during high performance (but unseeded) EDA H-mode discharges. As seen, the LHRF power fraction is considerably higher, qualitatively consistent with the ray-tracing/accessibility considerations indicating dominant deposition in boundary region. Another illuminating observation from the divertor heatflux measurements is the shape of the heatflux footprint on the target-plate. Both the peak heatflux and the total heatflux increase by a significant percentage of their target plasma values. However, the *profile shape* of the before- and during-LHRF footprints remains self-similar. This is shown in Fig. 8 and implies that the power reaching the divertor section viewed by the IR system is being deposited at or inside the separatrix, since the before-LHRF profile is determined by power flowing out through the separatrix into the SOL. We note, however, that SOL flux-tubes that pass in front of the LH

launcher are *not* magnetically connected to the section of the divertor plate where the footprint measurements are made. And, as we will see in the next section, there is some evidence for LH effects that *are* local to flux-tubes in the SOL that pass in front of the LH launcher. Thus some LHRF power may be deposited directly into

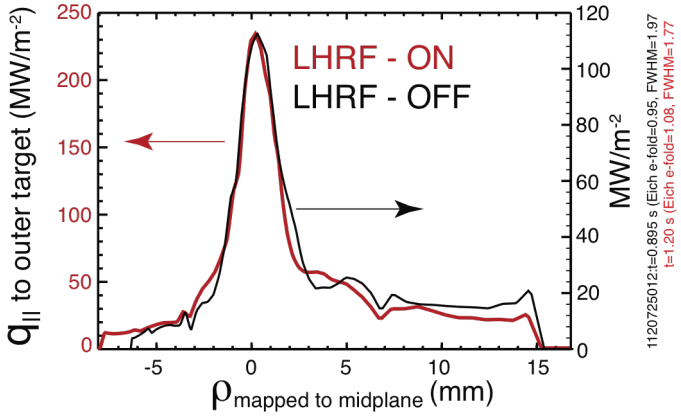

Figure 8. Profiles of the heat flux footprints on the instrumented section of the outer target, comparing the profile before the LHRF (black) to the profile during the LHRF-actuated confinement improvement (red). The left and right y-axis scales are configured such the profiles peaks align even though the peak heat flux is ~2x greater with the LHRF, so that it is apparent that the profile shape remains essentially the same. The x-axis is location on the outer target magnetically mapped to the outboard midplane, with ρ=0 defined as the separatrix.

the SOL on those SOL flux-tubes just in front of the launcher, and this power may not be detected by the thermography. Such a local LHRF power deposition has been seen previously in low-density L-mode plasmas[29].

Finally, as expected in these conditions, we find no evidence for LH current-drive in these plasmas. Neither of the two main diagnostics for LHCD detects changes indicative of current-drive. The multi-chord hard x-ray array [30], measuring bremsstrahlung emission from fast electrons, sees no change with the LHRF injection, nor is there evidence of non-thermal electron-cyclotron emission.

V. Turbulence Suppression with the Application of LHRF

Accompanying the confinement improvements with LHRF are large changes in (density) fluctuations in the plasma boundary. This is illustrated in Fig. 9, where spectrograms of density fluctuations from three different diagnostics (reflectometry [21], Phase Contrast Imaging (PCI) [21], and polarimetry [31]) are shown. Clearly evident is a strong perturbation to the Quasi-Coherent-Mode (QCM) which for the discharge of Fig. 9 has a before-LHRF frequency that is ~120 kHz and a during-LHRF frequency of ~60 kHz. The QCM is a well-studied mode, existing in the boundary region, that is primarily an electron drift-wave with interchange and electromagnetic contributions [32]. In EDA H-mode plasmas, which as noted are free of ELMs, the QCM is responsible for increasing the particle transport (relative to ELM-free, non-EDA H-modes) through the pedestal transport barrier, thereby allowing steady-state main-ion and impurity densities. The QCM frequency is typically in the 50-150 kHz range, with coherency such that $\Delta f/f_0^{QCM} \sim 0.05\text{-}0.15$; the mode is field aligned ($\vec{k} \bullet \vec{B} = 0$), with k_{pol}^{QCM} at the outer midplane typically around 1.5 cm^{-1}. Probe measurements during *Ohmic* H-modes show that the mode spans the separatrix in a region of positive E_r [32], but its exact location relative to the separatrix and to the E_r-

well is uncertain in these plasmas. (The plasmas under consideration here have too much boundary heat flux for scanning the probe near the separatrix.)

The effects of the LHRF-actuated pedestal changes on the QCM are:

- The central mode frequency (lab frame), f_0^{QCM}, decreases; if this is due to changes in **E**×**B** alone, then it means that E_r at the mode location increases and, therefore, that the mode does not live at the bottom of the E_r-well (see Section III).
- There is a small reduction or no change in poloidal wavenumber, k_{pol}^{QCM}; thus the phase velocity of the mode decreases.
- There is less temporal variation in f_0^{QCM}.
- $\Delta f/f_0^{QCM}$ typically decreases, i.e. coherency increases.

These changes are larger for larger ΔH_{98}. It is clear that these changes occur along with the pedestal profile and H_{98} changes, but it is not yet clear how they are connected.

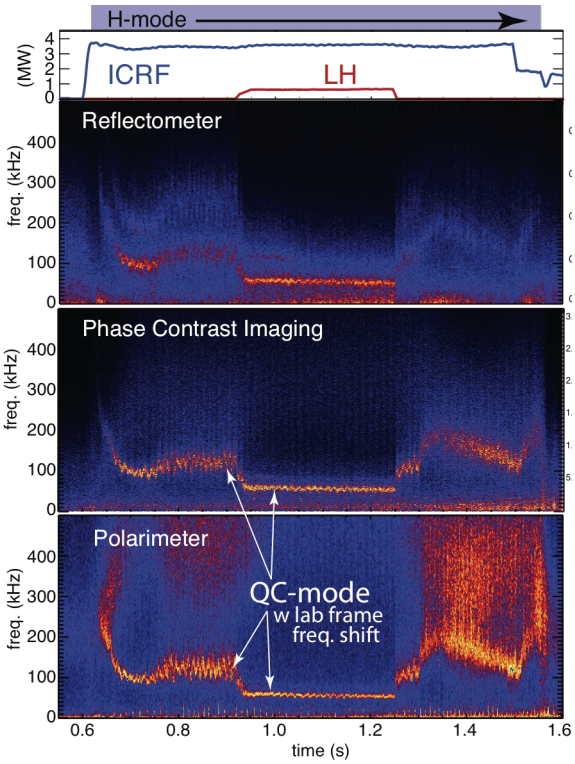

Figure 9. Spectrograms from three diagnostics sensitive to density fluctuations in the pedestal region. The large changes in the QCM and in the mid-frequency broadband turbulence during the LHRF-actuated confinement improvement are apparent. The ICRF and LHRF power waveforms are also shown.

Another change that is evident from the spectrograms of Fig. 9 is a decrease in broadband fluctuations in the ~100-300 kHz range with the LHRF-actuated confinement improvement. This is shown more quantitatively in Fig. 10(a), where spectra of density fluctuation power vs frequency are shown for time intervals before and during the LHRF. In order to investigate the correlation of this change in mid-frequency turbulence, we have removed the "contamination" of the QCM in this band by fitting it to a Gaussian, subtracting it from the spectrum, and then integrating the spectral power in the band. In Fig. 10(b) is plotted the change in

confinement vs the change in this integral, i.e. ΔH_{98} vs $\Delta \int_{100}^{300\,kHz} \tilde{n}_e^2(f)df$. As seen there is good correlation, with larger increases in ΔH_{98} occurring with larger *decreases* in mid-frequency turbulence. While this establishes a correlation, cause and effect are not determined. It is worth noting that C-Mod's I-mode plasmas also show decreases in mid-frequency density fluctuations and decreases in pedestal heat-transport coefficients compared to the L-mode target plasmas that precede them[33].

The decrease in mid-frequency fluctuations is seen by the diagnostics making chord integral measurements through the pedestal (PCI and polarimetry) as well as by

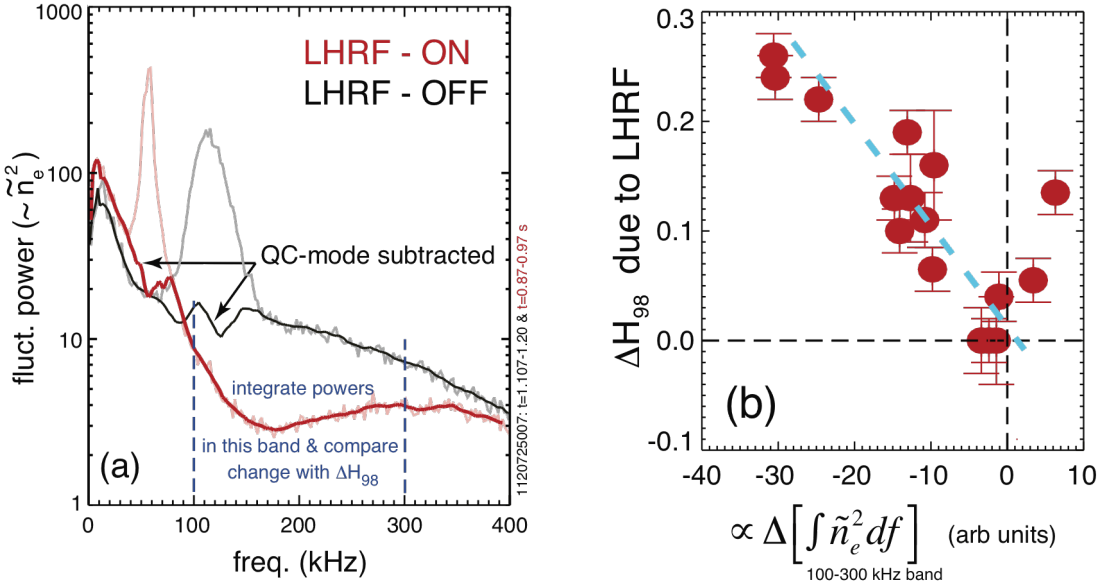

Figure 10. (a) Comparison of the power spectrum of density fluctuations vs frequency before and during the LHRF-actuated confinement improvement, as measured by PCI. It is a choral-measurement through core, pedestal, and SOL. In grey (light red) is the spectrum before (during) LHRF. In black (red) is the spectrum before (during) LHRF with the QCM contribution subtracted. (b) dependence of the confinement change, ΔH_{98}, on the change in the fluctuation power integrated on the 100-300 kHz band (with the QCM subtracted).

diagnostics that localize to the pedestal (reflectometry and Gas-Puff Imaging (GPI)), indicating that a decrease in *pedestal* turbulence is occurring with the pedestal profile modifications and confinement improvement. The GPI also images in the SOL and measures very large (~x10) decreases in broadband fluctuations with the LHRF injection on those SOL views. These large decreases are better-correlated with the LHRF itself than with the confinement change. This is evident in those cases where ΔH_{98} is small or zero, but the LHRF is on, and GPI still sees large decreases in the SOL fluctuations. This behavior contrasts with that of the pedestal fluctuations, which are better correlated with ΔH_{98} (as seen for example in Fig. 10(b)). It is also in contrast to what is observed by a Langmuir probe [32], positioned in these discharges just beyond the shadow of an outboard limiter. The probe sees no obvious change in $\tilde{I}_{sat}$ or $\tilde{V}_{float}$ with the LHRF. Since the GPI is such that it views SOL flux tubes that pass in front of the LH launcher (~48° away toroidally), while the probe samples a flux tube that does *not* pass in front of the launcher, we reconcile these apparently disparate observations by hypothesizing that *in the SOL* the LHRF modifies the turbulence on flux tubes local to the launcher.

VI. Connections with Observations of H-mode Plasmas without LHRF

In this section we examine the present observations within the context of previous studies of EDA H-mode plasmas in which there was no LHRF. Using a thoroughly analyzed set of impurity-seeded and unseeded EDA H-mode plasmas, Hughes, et al.[11] and Loarte, et al.[12] found that the H_{98}–factors were well ordered using the

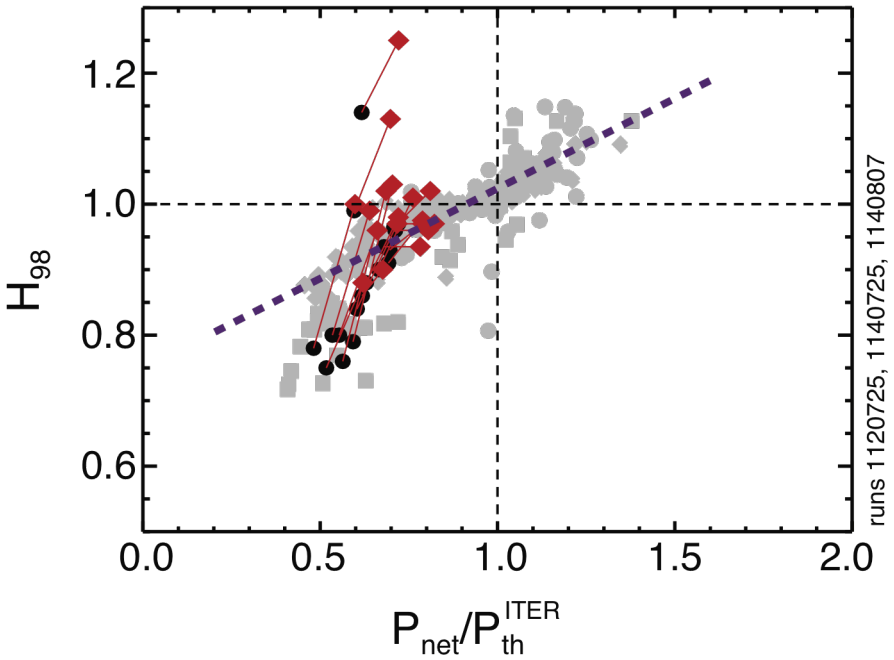

Figure 11. Trajectories of the H_{98}-factor vs P_{net} normalized by the ITER L-H power threshold (see text) during the LHRF-actuated confinement improvements. The black circles are the before-LHRF values, and the red squares are the maximum values during the LHRF. In the calculation of P_{net} it was assumed the 0.5 of P_{LHRF} is being deposited inside of the top of the pedestal. The grey points are from a data set of EDA H-modes without LHRF. The grey points have been filtered for cases with $n_{e,sep}/n_e^{bar} < 0.5$.

parameter P_{net} normalized by the L-to-H-mode threshold power, P^{ITER}_{th}, where P^{ITER}_{th} is evaluated according to the so-called ITER scaling [34]. P_{net} is the power flowing through the top of the pedestal and is calculated as P^{heat}_{core}-P^{rad}_{core}-dW/dt. When plotting H_{98} vs P_{net}/P^{ITER}_{th}, it was seen that the best H-modes clustered along the dashed line shown in Fig. 11 (These are the gray points in Fig. 11; see also Fig. 5 in ref [11]). Notably, for values of P_{net}/P^{ITER}_{th} >1, a number of discharges had significantly lower H_{98} than those fit by the dashed line. These underperforming discharges were found to have relatively large values of separatrix density and a significant portion of the H-mode density pedestal falling on open field lines. Confinement was satisfactory provided the electron density at the separatrix normalized by the line average density, $\frac{n_{e,sep}}{\bar{n}_e}$, was smaller than 0.5. Plasmas with smaller $\frac{n_{e,sep}}{\bar{n}_e}$ at similar P_{net}/P^{ITER}_{th} tended to have better confinement, while those with higher $\frac{n_{e,sep}}{\bar{n}_e}$ exhibited a degraded T_e pedestal and consequently a reduced H_{98}. Refs [11] and [12] considered plasmas *without* LHRF-actuated confinement

improvements. In Fig. 11 we also plot the trajectories of the LHRF-actuated plasmas under consideration here. The black circles are the before-LHRF values, and the connected red squares are the during-LHRF values. When we examine the change in the pedestal density profiles for the LHRF-actuated plasmas (as illustrated in the second panel of Fig. 3 where $\frac{n_{e,sep}}{\bar{n}_e}$ drops from 0.52 to 0.29 with the LHRF), we find a trend similar to that found in the H-modes with no LHRF, i.e. confinement improvements are positively correlated with reductions in $\frac{n_{e,sep}}{\bar{n}_e}$. The difference between the present observations and the previous ones is that with the LHRF we are actively changing this parameter using the LHRF actuator. As with the observation of correlation with turbulence reduction, we cannot assign cause and effect to the correlation with $\frac{n_{e,sep}}{\bar{n}_e}$, noting only for now the commonality and pointing out the probable importance of that quantity.

VII. Discussion and Summary

While we have demonstrated and described the use of LHRF to improve confinement by actuating changes in the pedestal, we do not have a clear understanding of *how* the LHRF actually causes these changes. That remains a work in progress. It is difficult to untangle the roles of the edge quantities that are changing with the LHRF injection. Edge turbulence, the QCM, the radial electric field, $\frac{n_{e,sep}}{\bar{n}_e}$, rotation are all changing, but which changes are primary causes and which are secondary effects is still unknown. Critical gradients in the edge profiles are known to exist [35,36], and they may be playing a role in these cases. The prompt power being supplied to the SOL by the LHRF can influence the neutral fueling both in H-mode and in L-mode, and this too is known to affect confinement [35,18].

We can only speculate about connections between these results and those found in reference [6], where LH power (with the dominant $n_{//}$ of the launched LH waves ranging from 1.9 to 2.8) was applied in C-Mod to lower-density EDA H-modes. Some differences in those target plasmas, compared to the ones considered here, are noteworthy: lower densities (1.5-2x10^{20} m^{-3} compared to 2.5-3.4x10^{20} m^{-3}), lower plasma currents (0.45 and 0.6 MA compared to 0.82 MA), DN or slightly USN configuration, a higher P_{LHRF}/P_{tot} fraction. While the pedestal pressure profiles were essentially unchanged and the global confinement was not significantly improved, other changes are qualitatively similar to those reported here, in that plasma density (pedestal and core) dropped along with increases in plasma temperature. Changes in core rotation were also observed in both data sets, although in different directions. In the lower-density H-modes the pedestal density gradient was reduced, implying increased particle transport there. In the improved-confinement plasmas considerd here the density drop at the separatrix is larger then that at the pedestal top, suggesting that perhaps the decreased accessibility of the LHRF may facilitate a drop in $\frac{n_{e,sep}}{\bar{n}_e}$ and an increase in pressure gradient.

In Section II we noted that the confinement improvement was reduced as the quality of the target plasma improved, as represented by the H_{98}-factor approaching 1. That is perhaps not surprising since $H_{98} \approx 1$ represents a general, but soft, "limit" for good EDA H-modes. The softness of the "limit" is clearly seen in Fig. 11 for values of P_{net}/P^{ITER}_{th} >1, and H_{98}-factors well above 1 are seen on other devices as

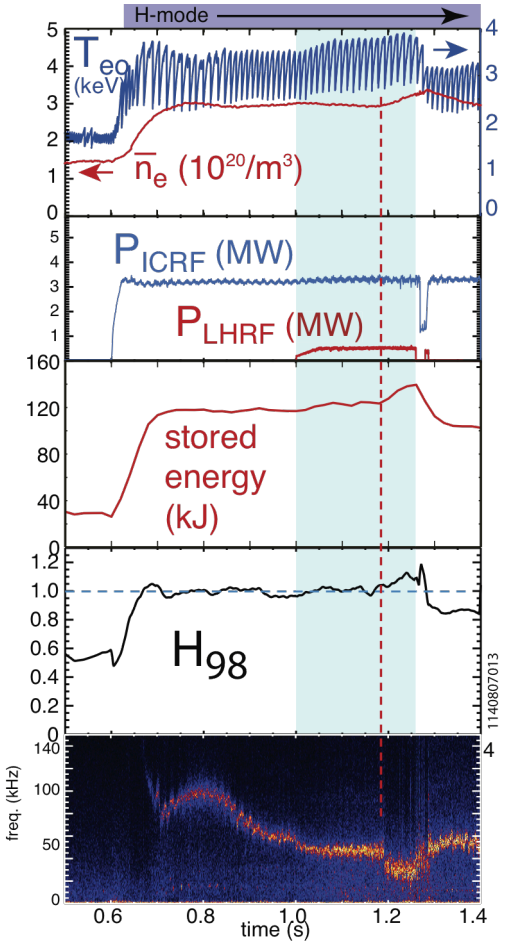

Figure 12. Time histories of line-averaged n_e and central T_e (top panel), ICRF and LHRF heating powers (2nd panel), plasma stored energy (3rd panel), H_{98}-factor (4th panel), and n_e fluctuations measured by PCI (bottom panel) for a LHRF-actuated H-mode in which the confinement of an H_{98}~1 was improved slightly during the 1st part of the LHRF pulse and then at ~1.2 s (red dashed line) went into a higher confinement condition. Note the break-in-slope of the density and stored energy, and the sharp decrease in the QCM frequency. The QCM is also changing its spatial structure at this time.

well as on C-Mod. Nonetheless, given the trend seen in Fig. 5, it is worthwhile to examine those few cases where the LHRF raised the H_{98}-factor from values >0.95 to values >1.1. In those instances there is evidence that new/different changes are occurring. Three differences from the more typical LHRF-actuated cases are seen: the density *increases* coincident with the confinement improvement, the spatial structure of the QCM changes (instead of remaining roughly the same), and the mid-frequency density fluctuations increase somewhat (instead of decreasing). These effects are shown in Fig. 12, where it is also apparent that the change to H_{98}=1.1 occurs rather late in the LHRF injection. At ~1.2 s (already 0.2 s into to the LHRF pulse), the QCM frequency decreases step-like to ~30 kHz as the QCM poloidal wavenumber drops by a factor of 0.67 and its toroidal mode number drops by approximately the same factor (from 18+/-2 to 13+/-1). At the same time the

density, stored energy, pedestal T_e, neutron rate begin to increase, and, in contrast to the cases examined earlier, quasi-stationary phases were not observed. The density fluctuation change shows an increase even though the H-factor is also increasing (this is represented by the right-most point in Fig. 10(b)). These cases motivate further investigation of these new effects using a larger data set.

To summarize the primary findings of this work: we have significantly increased global confinement by adding moderate levels of LHRF power to high-density H-mode plasmas. The improvements are brought about via modification of the pedestal, where electron pressure gradients are increased and the pedestal E_r-well is deepened. We have shown that these LHRF-actuated improvements are well correlated with suppressed pedestal turbulence in the 100-300 kHz range. There is also evidence that turbulence in the SOL is decreased locally on flux tubes that pass in front of the LH launcher. We have also pointed to a correlation between the improved confinement and a drop in $\frac{n_{e,sep}}{\overline{n}_e}$, a correlation that is consistent with previous H-mode results with no LHRF. The observed modifications occur without any evidence of current being driven by the LH. The LHRF power appears to be deposited in plasma boundary region, with large fraction of the injected power appearing promptly on outer divertor target. The profile *shape* of the power footprint on the outer target remains unchanged, at least on that section of the divertor where the measurement is made. However, since that divertor target section does not intercept SOL flux tubes passing in front of the LH launcher, the unchanged footprint shape does not preclude power deposition that is local to those flux tubes. Overall, we conclude that LHRF is being used as an actuator in these plasmas to affect global confinement via modification of quantities at the plasma edge. Not only does this actuator improve performance, but it also facilitates study and understanding of the edge as a boundary condition for the core.

Acknowledgments

This material is based upon work supported by the U.S. Department of Energy, Office of Science, Office of Fusion Energy Sciences, under Award Numbers DE-FC02-99ER54512 and DE-AC02-09CH11466 and in part by an appointment to the US DOE Fusion Energy Postdoctoral Research Program administered by ORISE.

References

[1]Y. Peysson, J. M. Ane, T. Aniel, G. Antar, J. F. Artaud, S. Balme, V. Basiuk, M. Basko, P. Bayetti, B. Beaumont et al., Nucl Fusion 41, 1703 (2001).

[2]A. Ekedahl, M. Goniche, D. Guilhem, F. Kazarian, and Y. Peysson, Fusion Science and Technology 56, 1150 (2009).

[3]J. R. Wilson, R. Parker, M. Bitter, P. T. Bonoli, C. Fiore, R. W. Harvey, K. Hill, A. E. Hubbard, J. W. Hughes, A. Ince-Cushman et al., Nucl Fusion 49, 115015 (2009).

[4]B.J. Ding, E. Kong, M. Li, Y. Qin, L. Zhang, A. Ekedahl, Y. Peysson, M. Wang, H. Xu, H. Hu et al., Plasma Science and Technology 13, 153 (2011).

[5]H. Ohtsuka, K. Hoshino, S. Kasai, T. Kawakami, H. Kawashima, H. Maeda, T. Matsuda, H. Matsumoto, M. Miura, M. Mori et al., Nucl Fusion 33, 523 (1993).

[6]J. W. Hughes, A. E. Hubbard, G. Wallace, M. Greenwald, B. LaBombard, L. Lin, R. M. McDermott, R. R. Parker, M. L. Reinke, J. E. Rice et al., Nucl Fusion 50, 064001 (2010).

[7]Y. Liang, X. Z. Gong, K. F. Gan, E. Gauthier, L. Wang, M. Rack, Y. M. Wang, L. Zeng, P. Denner, A. Wingen et al., Phys Rev Lett 110, 235002 (2013).
[8]M. Greenwald, Plasma Physics and Controlled Fusion 44, 27 (2002).
[9]J. D. Strachan, D. K. Mansfield, M. G. Bell, J. Collins, D. Ernst, K. Hill, J. Hosea, J. Timberlake, M. Ulrickson, J. Terry et al., J Nucl Mater 217, 145 (1994).
[10]H. W. Kugel, M. G. Bell, H. Schneider, J. P. Allain, R. E. Bell, R. Kaita, J. Kallman, S. Kaye, B. P. LeBlanc, D. Mansfield et al., Fusion Eng Des 85, 865 (2010).
[11]J. W. Hughes, A. Loarte, M. L. Reinke, J. L. Terry, D. Brunner, M. Greenwald, A. E. Hubbard, B. LaBombard, B. Lipschultz, Y. Ma et al., Nucl Fusion 51, 083007 (2011).
[12]A. Loarte, J. W. Hughes, M. L. Reinke, J. L. Terry, B. LaBombard, D. Brunner, M. Greenwald, B. Lipschultz, Y. Ma, S. Wukitch et al., Phys Plasmas 18, 056105 (2011).
[13]P. T. Bonoli, R. Parker, S. J. Wukitch, Y. Lin, M. Porkolab, J. C. Wright, E. Edlund, T. Graves, L. Lin, J. Liptac et al., Fusion Science and Technology 51, 401 (2007).
[14]R. Parker, P. T. Bonoli, O. Meneghini, M. Porkolab, A. E. Schmidt, S. Shiraiwa, G. Wallace, J. R. Wilson, A. E. Hubbard, J. W. Hughes et al., Radio Frequency Power in Plasmas 1187, 319 (2009).
[15]S. Shiraiwa, O. Meneghini, R. R. Parker, G. Wallace, J. Wilson, I. Faust, C. Lau, R. Mumgaard, S. Scott, S. Wukitch et al., Nucl Fusion 51, 103024 (2011).
[16]M. Greenwald, N. Basse, P. Bonoli, R. Bravenec, E. Edlund, D. Ernst, C. Fiore, R. Granetz, A. Hubbard, J. Hughes et al., Fusion Science and Technology 51, 266 (2007).
[17]B. Lipschultz, Y. Lin, M. L. Reinke, A. Hubbard, I. H. Hutchinson, J. Irby, B. LaBombard, E. S. Marmar, K. Marr, J. L. Terry et al., Phys Plasmas 13, 056117 (2006).
[18]M. L. Reinke, J. W. Hughes, A. Loarte, D. Brunner, I. H. Hutchinson, B. LaBombard, J. Payne, and J. L. Terry, J Nucl Mater 415, S340 (2011).
[19]ITER-Physics-Basis:Chapter-2, Nucl. Fusion 39, 2175 (1999).
[20]J. E. Rice, Y. A. Podpaly, M. L. Reinke, C. Gao, S. Shiraiwa, J. L. Terry, C. Theiler, G. M. Wallace, P. T. Bonoli, D. Brunner et al., Nucl Fusion 53, 093015 (2013).
[21]N. P. Basse, A. Dominguez, E. M. Edlund, C. L. Fiore, R. S. Granetz, A. E. Hubbard, J. W. Hughes, I. H. Hutchinson, J. H. Irby, B. LaBombard et al., Fusion Science and Technology 51, 476 (2007).
[22]R. J. Groebner, D. R. Baker, K. H. Burrell, T. N. Carlstrom, J. R. Ferron, P. Gohil, L. L. Lao, T. H. Osborne, D. M. Thomas, W. P. West et al., Nucl Fusion 41, 1789 (2001).
[23]R. M. Churchill, C. Theiler, B. Lipschultz, R. Dux, T. Putterich, E. Viezzer, Alcator C-Mod Team, and ASDEX Upgrade Team, Rev Sci Instrum 84, 093505 (2013).
[24]C. Theiler, R. M. Churchill, B. Lipschultz, M. Landreman, D. R. Ernst, J. W. Hughes, P. J. Catto, F. I. Parra, I. H. Hutchinson, M. L. Reinke et al., Nucl Fusion 54, 083017 (2014).
[25]R. M. McDermott, B. Lipschultz, J. W. Hughes, P. J. Catto, A. E. Hubbard, I. H. Hutchinson, R. S. Granetz, M. Greenwald, B. LaBombard, K. Marr et al., Phys Plasmas 16, 056103 (2009).
[26]M. Brambilla, *Kinetic Theory of Plasma Waves: Homogeneous Plasmas* (Oxford University Press, Oxford, 1998).
[27]R.W. Harvey and M. McCoy, Proceedings of the IAEA Technical Committee Meeting on Simulation and Modeling of Thermonuclear Plasmas 1992 (pp. 489–526).
[28]J. L. Terry, B. Labombard, D. Brunner, J. Payne, and G. A. Wurden, Rev Sci Instrum 81, 10E513 (4 pp.) (2010).
[29]A. N. James, D. Brunner, B. Labombard, C. Lau, B. Lipschultz, D. Miller, M. L. Reinke, J. L. Terry, C. Theiler, G. M. Wallace et al., Plasma Physics and Controlled Fusion 55, 125010 (2013).
[30]J. Liptac, R. Parker, V. Tang, Y. Peysson, and J. Decker, Rev Sci Instrum 77, 103504 (2006).
[31]W. F. Bergerson, P. Xu, J. H. Irby, D. L. Brower, W. X. Ding, and E. S. Marmar, Rev Sci Instrum 83, 10E316 (2012).
[32]B. LaBombard, T. Golfinopoulos, J. L. Terry, D. Brunner, E. Davis, M. Greenwald, J. W. Hughes, and Alcator C-Mod Team, Phys Plasmas 21, 56108 (2014).
[33]A. E. Hubbard, D. G. Whyte, R. M. Churchill, I. Cziegler, A. Dominguez, T. Golfinopoulos, J. W. Hughes, J. E. Rice, I. Bespamyatnov, M. J. Greenwald et al., Phys Plasmas 18, 056115 (2011).
[34]Y. R. Martin, T. Takizuka, and ITPA CDBM H-Mode Threshold Database Working Group, J Phys Conf Ser 123, 012033 (2008).
[35]J. W. Hughes, B. LaBombard, J. Terry, A. Hubbard, and B. Lipschultz, Nucl Fusion 47, 1057 (2007).

[36]**B. LaBombard, J. W. Hughes, N. Smick, A. Graf, K. Marr, R. McDermott, M. Reinke, M. Greenwald, B. Lipschultz, J. L. Terry et al., Phys Plasmas 15 (2008).**